

# Scholar@UPRM

## Molecular simulations of model Langmuir monolayers

Item Type	Thesis
Authors	Villalobos Rivera, Leslie V.
Download date	2026-05-14 07:08:26
Link to Item	<a href="https://hdl.handle.net/20.500.11801/3821">https://hdl.handle.net/20.500.11801/3821</a>

# Molecular Simulations of model Langmuir Monolayers

by

**Leslie V. Villalobos Rivera**

A thesis submitted in partial fulfillment  
of the requirements for the degree of

**Master of Science  
in  
Chemistry**

University of Puerto Rico  
Mayagüez Campus  
**2005**

Approved by:

\_\_\_\_\_  
Astrid J. Cruz Pol, Ph.D.  
Member, Graduate Committee

\_\_\_\_\_  
Date

\_\_\_\_\_  
Francis Patrón, Ph.D.  
Member, Graduate Committee

\_\_\_\_\_  
Date

\_\_\_\_\_  
Gustavo E. López Quiñones, Ph.D.  
President, Graduate Committee

\_\_\_\_\_  
Date

\_\_\_\_\_  
Carlos Rinaldi, Ph.D.  
Representative of Graduate Studies

\_\_\_\_\_  
Date

\_\_\_\_\_  
María Aponte, Ph.D.  
Chairperson of the Department

\_\_\_\_\_  
Date

## Abstract

The study of Langmuir monolayers has generated the attention of researchers because of their unique properties and their not well understood phase equilibrium. These monolayers exhibit interesting phase diagrams where the unusual liquid-liquid equilibrium can be observed for a single component monolayer submitted to an external applied pressure. In this study, the thermodynamic properties of a model Langmuir monolayer were determined using two types of computer simulations. First, Monte Carlo simulations in the Isothermal-Isobaric ensemble were used to obtain adsorption isotherms of Langmuir monolayers. The results clearly show coexistence of two liquid phases, denominated as liquid expanded state (LES) and liquid condensed state (LCS). Radial distribution function and distribution functions of enthalpies for the monolayer were also computed to clearly identify each liquid phase and the coexistence region. A second model was used to obtain the critical properties for this model system. The phase equilibrium between the liquid phases and the LES-Vapor (V) phases has been considered using Monte Carlo computer simulations in the Standard Virtual Gibbs Ensemble. The Caillete- Mathias phase diagrams were constructed and two models were implemented in order to determine the critical parameters of the system. Specifically, the Ising Model and the rectilinear approximation were used to identify the critical temperature ( $T_c^*$ ) and the critical density ( $\rho_c^*$ ), respectively. These critical parameters were identified by varying the interaction between the surfactant molecules and the aqueous phase. Finally, we have identified the coexistence between the LES and LCS states, in agreement with experimental and theoretical evidence in the literature. Furthermore, we have successfully identified the critical parameters  $T_c^*$  and  $\rho_c^*$  for the LES-LCS and the LES-V equilibrium of the monolayer.

## Resumen

El estudio de las monocapas de Langmuir ha generado el interés de la comunidad científica debido a que presentan un comportamiento termodinámico no esperado para un sistema de un solo componente. Estas monocapas poseen diagramas de fase donde se observa que al aplicársele una presión externa es posible identificar la presencia de un equilibrio entre dos fases líquidas denominadas como líquida expandida (LES) y líquida condensada (LCS). En este trabajo, las propiedades termodinámicas de la monocapa de Langmuir fueron determinadas utilizando dos tipos de simulaciones en computadora. El primer colectivo utilizado fue el isotermico-isobárico para obtener las isotermas de adsorción de la monocapa de Langmuir. Estas isotermas muestran claramente la coexistencia de las dos fases líquidas. Además, se calculó la función de distribución de entalpía y la función de distribución radial para identificar de una forma más clara las fases líquidas de la monocapa y la región de coexistencia entre ellas. El segundo modelo se utilizó para determinar las propiedades críticas de las fases LES-LCS y LES-Vapor (V) utilizando una simulación de Monte Carlo en el colectivo Estándar Virtual de Gibbs. Para determinar los parámetros críticos de las fases en equilibrio estudiadas se aplicaron dos modelos a los diagramas de fase de Caillette-Mathies. Específicamente, el modelo de Ising y la aproximación rectilínea se utilizaron para identificar la temperatura crítica ( $T_c^*$ ) y la densidad crítica ( $\rho_c^*$ ), de las fases en equilibrio respectivamente. Estos parámetros críticos fueron identificados variando la interacción entre los surfactantes que forman la monocapa de Langmuir y la fase acuosa. La coexistencia entre las fases LES y LCS se logró identificar utilizando el método previamente mencionado. Los resultados obtenidos reflejan el comportamiento de la monocapa de Langmuir descrito por estudios previos. Mas aún, se identificaron las propiedades críticas  $T_c^*$  y  $\rho_c^*$  para los equilibrios entre las fases LES-LCS y LES-V.

## **Acknowledgments**

I am very grateful to those who collaborated with me in this period of my life. Special thanks to my advisor Dr. Gustavo López for his guidance and patience. Also thanks to my graduate committee members, Dr. Astrid Cruz and Dr. Francis Patrón. Thanks to my colleague and friend Johnny Maury for his unconditional help and encouragement. Special thanks to the people in the Theoretical and Computational Chemistry group Laboratory, especially to Yania M. López. I would like to thank Angélica, Ariel, Kawille, Lourdes, María, Yahaira, and Yessenia for being wonderful friends and for their help and support. I wish to acknowledge Dr. Juan López Garriga for the opportunity to work as a GUEST K-12 Fellow. Thanks to my friends in the Science on Wheels Educational Center, mostly to Ricardo Camacho and Lisa M. Betancourt for their invaluable advice and for being great role models. I am most indebted to my family, especially to my parents Carlos J. Villalobos and Josefina Rivera for their understanding and being the best example of unselfish love. To them I dedicate this accomplishment with all my love.

# Table of Contents

List of Tables	vi
List of Figures	vii
<b>1. Introduction</b>	<b>1</b>
1.1 Motivation	1
1.2 Literature Revision	4
1.3 Brief Outline	6
<b>2. Thermodynamics of the liquid states of Langmuir monolayers</b>	<b>8</b>
2.1 Model	10
2.1.1 Interparticle potential	10
2.2 Method	11
2.2.1 Monte Carlo Technique in Isothermal–Isobaric Ensemble	12
2.3 Simulation Details	14
2.4 Thermodynamic Properties	17
2.5 Results and Discussion	18
2.6 Conclusions	28
<b>3. Langmuir monolayer Critical Properties Determination</b>	<b>29</b>
3.1 Model	30
3.1.1 Interparticle potential	30
3.2 Method	31
3.2.1 Monte Carlo Technique in the Standard Virtual Gibbs Ensemble	32 32
3.3 Simulation Details	33
3.4 Results and Discussion	35
3.5 Conclusions	46
<b>4. General Conclusions</b>	<b>47</b>
<b>References</b>	<b>49</b>

## List of Tables

Table 1. Parameters for the repulsive and attractive parts of the Lennard-Jones Interparticle potential	11
Table 2. Langmuir Monolayer critical properties for the LES-LCS equilibrium and the LES-V equilibrium. The critical temperature and density are reported in reduced units.	45

## List of Figures

Figure 1: Schematic representation of the molecular model used to study the Langmuir monolayer	9
Figure 2: Snapshot of the model Langmuir monolayer	16
Figure 3: Lateral spreading pressure as a function of average surface area per atom at constant temperature (adsorption isotherm) for a Langmuir monolayer	19
Figure 4: Average enthalpy per atom as a function of pressure at constant temperature for a Langmuir monolayer	21
Figure 5: Distribution function of distances between pairs as a function of distance between pairs of the Langmuir monolayer for a solid-like computed at $\Pi^* = 50$ and $T^* = 1.0$ and for a vapor-like computed at $\Pi^* = 1$ and $T^* = 7.0$	23
Figure 6: Distribution function of distances between pair as a function of distance between pairs of the Langmuir monolayer for the LES, LCS and the LES-LCS equilibrium computed at $T^* = 2.0$ and $\Pi^* = 25, 40$ and $33$ , respectively	24
Figure 7: Snapshots of equilibrium configurations corresponding to (a) LCS, (b) LES, and (c) LES-LCS equilibrium. The snapshots were constructed plotting only the head of the surfactant molecule in the x-y plane and drawing a bond between next-nearest neighbors	25
Figure 8: Distribution Function of Enthalpies as a function of enthalpies of the Langmuir monolayer at $T^* = 2.0$ and lateral applied pressure of (a) 25 (b) 40 and (c) 33	27
Figure 9: Caillette-Matties phase diagram for the Langmuir monolayer at three different interaction values.	36
Figure 10: For $\varepsilon = 1$ (a) Reduced temperature as a function of $(\rho_1 - \rho_2)^3$ for the LES-LCS equilibrium (b) Rectilinear law implementation for the critical density identification. The straight line represents a least- square fit to the simulation results.	38

- Figure 11: For  $\varepsilon = 10$  (a) Reduced temperature as a function of  $(\rho_1 - \rho_2)^3$  for the LES-LCS equilibrium (b) Rectilinear law implementation for the critical density identification. The straight line represents a least- square fit to the simulation results. 39
- Figure 12: For  $\varepsilon = 50$  (a) Reduced temperature as a function of  $(\rho_1 - \rho_2)^3$  for the LES-LCS equilibrium (b) Rectilinear law implementation for the critical density identification. The straight line represents a least- square fit to the simulation results. 40
- Figure 13: For  $\varepsilon = 1$  (a) Reduced temperature as a function of  $(\rho_1 - \rho_2)^3$  for the LES-V equilibrium (b) Rectilinear law implementation for the critical density identification. The straight line represents a least- square fit to the simulation results. 42
- Figure 14: For  $\varepsilon = 10$  (a) Reduced temperature as a function of  $(\rho_1 - \rho_2)^3$  for the LES-V equilibrium (b) Rectilinear law implementation for the critical density identification. The straight line represents a least- square fit to the simulation results. 43
- Figure 15: For  $\varepsilon = 50$  (a) Reduced temperature as a function of  $(\rho_1 - \rho_2)^3$  for the LES-V equilibrium (b) Rectilinear law implementation for the critical density identification. The straight line represents a least- square fit to the simulation results. 44

# Chapter 1

## Introduction

### 1.1 Motivation

The study of surfactant molecular adsorption on aqueous phases is an important topic in both theoretical and experimental research due to its role in many biological and bioengineering processes. In general, surfactant molecules consist of a polar or hydrophilic head group and a non polar or hydrophobic tail. This structural pattern allows them to be employed as soaps, detergents, and in microelectronics, among other applications<sup>1</sup>. Physiologically, surfactants are present in many biological processes. Among these, surfactants help prevent the alveoli from collapsing by interfering with the cohesiveness of water molecules, thereby reducing the surface tension of alveolar fluid<sup>2</sup>. In fact, surfactant molecules are essential for the existence of life and hence it is impossible to consider any living processes without the participation of this kind of molecule.

When insoluble surfactants are present in an aqueous medium, the hydrophilic head group attaches to the water surface while the hydrophobic tail extends above the surface forming an air-water interface with the thickness of one molecule, known as Langmuir monolayer. Since century XIX, the study and understanding of Langmuir monolayers has made great advances. In biophysics, Langmuir monolayers have been studied as excellent models for membranes, since a biological membrane consists of two coupled monolayers<sup>3</sup>. Also, the understanding of the adsorption of proteins to biological membranes plays a critical role in biochemical processes within living systems. One of the main difficulties that scientists are investigating is the behavior of proteins when they are incorporated into amphiphilic monolayers at the air-water interface<sup>4</sup>.

From a physical perspective, the major issue of Langmuir monolayers is the prediction and understanding of their thermodynamic properties. The main source of experimental thermodynamic data of Langmuir monolayers is acquired from Surface Pressure–Area Isotherms. These isotherms show a number of distinct regions that correspond to the two dimensional analogues of the monolayer usual states<sup>5-7</sup>. Various studies have reported isotherms where a number of states and the equilibrium between them have been clearly identified as the monolayer is compressed<sup>7-9</sup>. When the area per molecule is very large, the monolayer is in a vapor phase (V). Isothermal compression generates a transition from the vapor phase to a liquid expanded state (LES). Further

isothermal compression of the monolayer generates the transition from the LES to a liquid state of greater values of density known as the liquid condensed state (LCS)<sup>10</sup>. Experimental studies<sup>11-13</sup> have shown the existence of a region of liquid-liquid equilibrium between LES and LCS that has been characterized by applied lateral pressure vs. surface area isotherms. This transition, and the resulting coexistence of two or more states, are phenomena not fully understood and, thus, are the main impetus for the continued study of the behavior of Langmuir monolayers.

Since many of the studies done on Langmuir monolayers have focused on their macroscopic properties, there is a lack of information about such layers at a molecular level. Computer simulations have become a useful tool to study complex materials such as surfactant layers and provide a mean of interpreting experimental data in terms of molecular properties. For instance, some particular features of structure and phase behavior of Langmuir monolayers can be understood using computer simulations. Specifically, Monte Carlo simulations can be used to explain the effect of chain length on monolayer properties, as well as to study Langmuir monolayer phase equilibrium and the differences between the structure and properties of monolayers formed in different aqueous phases. For a better understanding and better interpretation of the behavior of Langmuir monolayers, it is therefore important to study the thermodynamics of the various monolayer phases and the phase equilibrium between the different monolayer states.

## 1.2 Literature Revision

Phase transitions in Langmuir monolayers vary most significantly, with respect to the monolayer material, hydrophobic chain length, and density<sup>14-15</sup>. It has been found that the monolayer experiences the same sequence of phase transitions, but at different intervals of temperature and pressure. Specifically, longer molecules with the same head group, experience phase transitions at higher temperatures than molecules with shorter hydrocarbon chains<sup>16</sup>. In addition, the interaction between head groups can be varied by changing the pH of the subphase, as is shown by Castillo et al.<sup>17</sup> They have demonstrated that the phase transitions and phase equilibrium of the monolayer formed with dioctadecylamine depends on the aqueous subphase pH value. There is also some analogy between the behavior of some phospholipids at the air-water interface and the pH of the subphase. Protonation of the head group leads to more expanded monolayers due to the electrostatic interactions between them. It is also known that increasing ionic strength by addition of salts with counter ions in the subphase induces a condensation of the monolayer.

Several computational methods have been used to investigate some of the characteristics of Langmuir monolayers<sup>18-20</sup>. To study structural details, thermodynamic properties, and the phase behavior of Langmuir monolayers, investigators have used several specialized methods to simulate corresponding experimental systems as closely as possible. Particularly, Monte Carlo simulations were used to study the different kinds of liquid phases exhibited by a

Langmuir monolayer<sup>7</sup>. The molecular models were based on descriptions of the surfactant molecules as semi-rigid rods where the head and tail consist of monomers representing various groups. Similarly, the interactions between the monomers were described by Lennard-Jones potentials. This model was used by Opps et al.<sup>7</sup> using constant molecule number, surface area, and temperature simulations. They observed that when the diameters of the tail monomers are less than the head monomers, the surfactant goes through a reorientation and a decrease in the critical temperature is observed as a result of the increase in the orientational entropy. Additionally, they found that an increase in head diameter causes a widening of the liquid/gas interface, which in turn affected the orientation of the surfactant molecules. In another study, Opps and his collaborators<sup>18</sup> considered the interaction among model surfactant molecules and a water surface. They found that at a fixed area per molecule, and with variations in the bond length to head diameter ratio, the conformational behavior of the Langmuir monolayer switched from an untilted phase to a tilted phase. Also, they discovered that, at the ground state, the behavior of the monolayer was affected by changes in the intramolecular bond length and the head diameter.

Using Molecular Dynamics simulations, Tomassone et al. have studied the surface tension and the surface concentration isotherms of a model surfactant system<sup>19</sup>. They reported that with an appropriate fixing of the Lennard-Jones potential it is possible to study the interaction between surfactants plus solvent

systems, their isotherms, and the phase transition properties. Also, they found that there is coexistence of the gas/liquid expanded phases when the attraction between the surfactant molecules and the solvent is increased. Hence, for insoluble systems the phase coexistence is commonly studied and a number of states can be clearly identified<sup>7,12,18-20</sup>.

### **1.3 Brief Outline**

As stated previously, there are many reasons to study Langmuir monolayers. In fact, a basic physical understanding of Langmuir monolayers is important when considering their applications in many fields of science and technology, such as chemistry, physics, material science and biology. For example, a thorough understanding of the monolayer behavior is essential for exploiting the Langmuir-Blodgett technique and to set up thin film materials with well defined structures to be applied in molecule-based electrical and optical devices<sup>21-23</sup>. Although much work has been done in this field, there still remain some unresolved issues pertaining to the thermodynamic properties and structural details of Langmuir monolayers.

Our goal in this work was to perform two kinds of Monte Carlo simulations in order to obtain a better description of Langmuir monolayer thermodynamic behavior. First, the isothermal-isobaric ensemble<sup>24</sup> was used in order to construct

adsorption isotherms (applied lateral pressure vs. monolayer average surface area) of the Langmuir monolayer. The simulations were designed to model, as closely as possible, the experimental set-up encountered in a Langmuir trough balance. The method allowed for the proper description of the water phase and the characterization of the LCS, LES, and the LCS-LES equilibrium.

In Langmuir monolayers formed of pure liquid system, the region of coexistence between the LES-V phases ends in a critical point. As far as we know, there is no evidence of a critical point for the region of coexistence between the LES-LCS phases in the literature<sup>3</sup>. The second model used in this work was the Standard Virtual Gibbs Ensemble<sup>24</sup> (SVGE). Specifically, the phase transitions between two liquid states and liquid-vapor state for the model system were studied using this ensemble. Cailletet- Mathias phase diagrams (T vs. density phase diagrams) for the model Langmuir monolayer were constructed and, as in previous studies<sup>25-26</sup>, the Ising model and the rectilinear law were used to determine the values of the critical temperature ( $T_c^*$ ) and the critical density ( $\rho_c^*$ ), respectively.

## **Chapter 2**

### **Thermodynamics of the liquid states of Langmuir monolayers**

#### **Model and Simulation Details**

The objective of this study was to characterize the phase transitions between two liquid phases in a Langmuir monolayer using Monte Carlo methods with a computational model that resembles the Langmuir–Adam trough experimental set-up. The equilibrium between LES–LCS was identified by constructing lateral pressure-surface area phase diagrams using the isothermal-isobaric ensemble where the number of particles, pressure, and temperature are constant. Furthermore, distribution functions of distances and enthalpies for the monolayer were computed to clearly identify each liquid phase and the coexistence range between them. A schematic representation of the simulation box used in this study is presented in Figure 1.

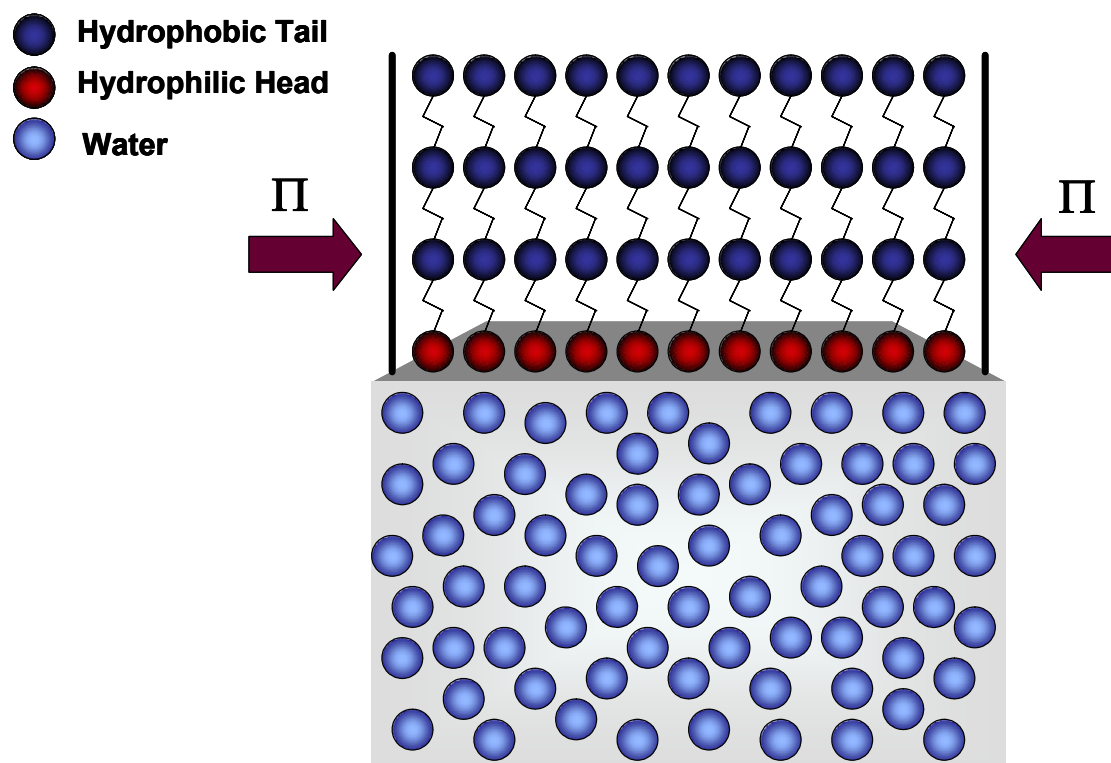


Figure 1: Schematic representation of the molecular model used to study the Langmuir monolayer

## 2.1 Model

### 2.1.1 Interparticle Potential

Surfactant chains were modeled using simple bead-like models<sup>27</sup>. All interactions between adjacent beads were described by harmonic oscillators of the form:

$$V_b(r_{ij}) = \frac{K}{2}(r_{ij} - \sigma)^2 \quad (1)$$

K is the force constant set to 500 units,  $r_{ij}$  is the distance between adjacent beads  $i$  and  $j$ , and  $\sigma$  is the equilibrium distance between beads, which was set to 1.0.

Interactions between the non-bonded beads were modeled using a modified 12-6 Lennard-Jones (L-J 12-6) potential<sup>28</sup> of the form:

$$\frac{V_{nb}(r_{ij})}{4\epsilon_{ij}} = R_{ij} \left( \frac{\sigma_{ij}}{r_{ij}} \right)^{12} - A_{ij} \left( \frac{\sigma_{ij}}{r_{ij}} \right)^6 \quad (2)$$

where  $V_{nb}(r_{ij})$  is the potential energy between non-bonded beads  $i$  and  $j$  at a separation of  $r_{ij}$ . The parameters  $\epsilon_{ij}$  and  $\sigma_{ij}$  are the usual L-J parameters and were set equal to 1.0. Hence, all quantities, including the temperature, were expressed in reduced units, e.g. reduced temperature,  $T^* = T/\epsilon_{ij}$ ,  $K^* = K\sigma_{ij}^2/\epsilon_{ij}$  and  $r_{ij}^* = r_{ij}/\sigma_{ij}$ . The constants  $R_{ij}$  and  $A_{ij}$  are used to modify the repulsive and attractive parts of the potential, respectively. Those parameters, which are defined in Table 1, are fixed in order to represent the different polarities in the

system. For example, the repulsive interactions between hydrophilic beads and hydrophobic beads are represented by fixing  $R_{ij} = 1.0$  and  $A_{ij} = 0$ . Each surfactant molecule was modeled by one bead representing the hydrophilic head and three beads representing the hydrophobic tail. The water molecules were modeled with an L-J potential with the parameters  $\epsilon_{ij}$  and  $\sigma_{ij}$  fixed to 1.0 and 0.8, respectively.

<b>INTERACTIONS</b>	<b><math>R_{ij}</math></b>	<b><math>A_{ij}</math></b>
Head-Head	1.0	1.0
Tail-Tail	1.0	1.0
Water-Water	1.0	1.0
Head-Tail	1.0	0.0
Head-Water	1.0	1.0
Tail-Water	1.0	0.0

Table 1: Parameters used for the repulsive  $R_{ij}$  and attractive  $A_{ij}$  parts of the interparticle potential.

## 2.2 Method

The thermodynamic properties of the liquid states of the model Langmuir monolayer were studied using the Metropolis Monte Carlo algorithm in the isothermal-isobaric ensemble, where the number of particles, the temperature, and the pressure are held constant (NPT ensemble) while the volume of the simulation box is allowed to fluctuate. This method is particularly appropriate for

simulating mixtures<sup>29</sup>, single component fluids<sup>30</sup> and has also been used in the study of phase transitions<sup>31</sup>. In this case the NPT ensemble was used to identify the phase equilibrium between the LES-LCS of the monolayer. Details on the method implemented are given in the next section.

### 2.2.1 Monte Carlo Technique in Isothermal–Isobaric Ensemble

In the standard Metropolis Monte Carlo algorithm a random walker samples the configuration space from an initial configuration  $q_i$  to a final configuration  $q_f$  with a probability of acceptance,  $P$ , which is given by

$$P = \min [1, a(q_f, q_i)] \quad (3)$$

Then the probability of acceptance of a new configuration is the minimum between 1.0 and  $a(q_f, q_i)$  is given by

$$a(q_f, q_i) = \frac{S(q_i|q_f) p(q_f)}{S(q_f|q_i) p(q_i)} \quad (4)$$

Here the quantity  $S(q_i|q_f)$  is the transition probability and  $p(q)$  is the distribution function, which in the Isothermal-Isobaric ensemble is given by

$$p(q) = \frac{\exp[-\beta U(q)]}{\Delta(N, \Pi, T)} \quad (5)$$

where  $U$  is the potential energy,  $\beta = 1/k_B T$ , ( $k_B$  is the Boltzmann constant and  $T$  is the absolute temperature) and  $\Delta(N, \Pi, T)$  is the partition function corresponding to the isothermal-isobaric ensemble and is given by

$$\Delta = \sum_i \exp[-\beta(U_i + \Pi A)] \quad (6)$$

The detailed balance condition<sup>32</sup> demands that, at equilibrium the transition probability of going from an initial configuration  $q_i$  to a final configuration  $q_f$  is equal to the transition probability of going from  $q_f$  to  $q_i$ . This can be expressed as

$$S(q_i | q_f) = S(q_f | q_i) \quad (7)$$

The substitution of this condition into equation 4 leads to

$$a(q_f, q_i) = \frac{p(q_f)}{p(q_i)} \quad (8)$$

Hence the transition probability distribution is given by

$$P = \min [1, \exp[-\beta \Delta U]] \quad (9)$$

Here  $\Delta U$  is the difference in configurational energy between the final and initial states.

As stated in section 2.2, for the identification of the equilibrium between two liquid phases, the surfactant molecules were simulated using the NPT ensemble where two moves were allowed on the monolayer. First, particle displacements were performed using the usual acceptance probability between final and initial states,  $P$ , given by equation 9.

The second type of move consisted of changes in the surface area of the surfactant monolayer and the corresponding acceptance probability was given by

$$P = \min[1, \exp[-\beta(\Delta U + \Pi \Delta A)]] \quad (10)$$

Here,  $\Delta A$  is the difference in area between the initial and the final states. The variation in area was performed in the x-y plane of the monolayer with rhombic arrangement, i.e. only the size of the sides of the box in the x-y plane was changed. The water molecules, which were placed below the monolayer, were not subjected to the applied lateral pressure ( $\Pi$ ). Hence, the only type of movement performed to the water molecules was particle displacement.

### 2.3 Simulation Details

Initially, the monolayer of surfactant molecules were placed in the x-y plane in a rhombic arrangement and with a lateral spreading pressure,  $\Pi$ , applied to the monolayer. The hydrophilic heads of the monolayer were placed in contact with a water bath and the hydrophobic tails in contact with air as shown in Figure 2.

Initially, the surfactant molecules were placed in a closed-packed arrangement with rhombic periodic boundary conditions and the water molecules in a random configuration at a density of approximately 1.0 g/ml. A total of 500 surfactant molecules and 9,232 water molecules were used in the simulations. Each surfactant molecule is composed of one bead representing the hydrophilic head bonded to three identical beads representing the hydrophobic tail. The initial size of the box in reduced units in the x-y plane was 50x50 and in the z direction for the water box was 5 reduced units. A reflective wall was used in the z direction for the surfactant molecules.

The simulations were run for a total of  $10^7$  warm-up moves and  $10^7$  moves where data was collected. The step sizes were adjusted in order to have an acceptance ratio for the particle displacement and box size variation of approximately 50% and 30%, respectively. Periodic boundary conditions were used in the x-y plane. In the z direction, at the bottom of the box, a reflective wall was used and in the top of the box no boundary was defined. Because the interaction between the surfactant and the water is relatively strong, no surfactant molecule was observed leaving the monolayer.

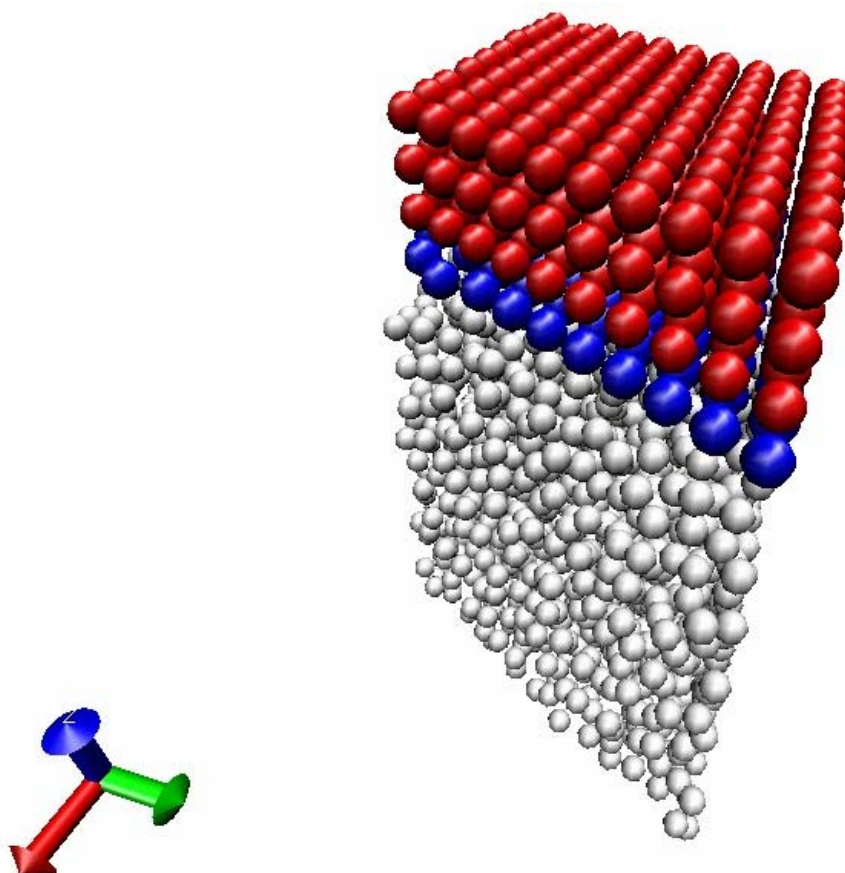


Figure 2: Snapshot of the model Langmuir monolayer

## 2.4 Thermodynamic Properties

The thermodynamic properties that can be obtained from simulations where the thermodynamic state is defined fixing the pressure and temperature are: enthalpy, constant pressure heat capacity ( $C_P$ ), isothermal compressibility and thermal expansion factors. In this work the characterization of the phase transitions was performed by computing the ensemble average surface area in the x-y plane at a given temperature and lateral pressure and constructing adsorption isotherms for the monolayer, i.e.  $\Pi$  vs.  $\langle A \rangle$  diagrams at fixed temperature. The average enthalpy,  $\langle H \rangle$ , of the monolayer was also computed using the expression:

$$\langle H \rangle = \langle U \rangle + \Pi \langle A \rangle \quad (11)$$

where  $\langle U \rangle$  is the average internal energy of the monolayer.

In order to obtain information related to the structural and thermodynamic changes occurring in the system, various distribution functions were computed. The calculation of the distribution function of reduced distance between pairs,  $P(r_{ij}^*)$  in Monte Carlo simulations is straightforward. All that has to be done is count the number of particles at the distance of  $r$  and  $r + dr$  from the chosen particle. The distribution function of reduced enthalpies,  $P(H^*)$  was also computed for the surfactant molecules. Both distribution functions were computed by constructing a histogram with the appropriate binning. It is expected that when the system has a single phase, the distribution function of

reduced enthalpies show a unimodal distribution, whereas for coexistence of phases, a bimodal distribution should be expected.

## 2.5 Results and Discussion

A system consisting of 500 surfactant molecules submitted to a lateral applied pressure was considered. The results from this study are presented in Figures 3-8. Figure 3 shows the adsorption isotherms for the Langmuir monolayer considered here at six different temperatures. It can be observed that at the highest temperature studied  $T^*=5.0$ , a typical single phase isotherm was obtained. As explained and corroborated, this phase corresponds to a liquid state with large separation between the surfactant molecules and high values of average enthalpy. Hence, this phase can be described as the LES. On the other hand, at the lowest temperature considered,  $T^*=0.8$ , the same behavior was observed; a single liquid phase was obtained but corresponding to a different liquid phase that can be characterized as a structurally compacted state denominated as the LCS. At intermediate temperatures,  $T^*=1.5, 2.0$  and  $3.0$ , three regions could be clearly identified. At low and high pressures, single phase regions were observed corresponding to the LES and the LCS, respectively. However, at intermediate pressures, a region could be identified where the pressure remained approximately constant as the average surface area of the

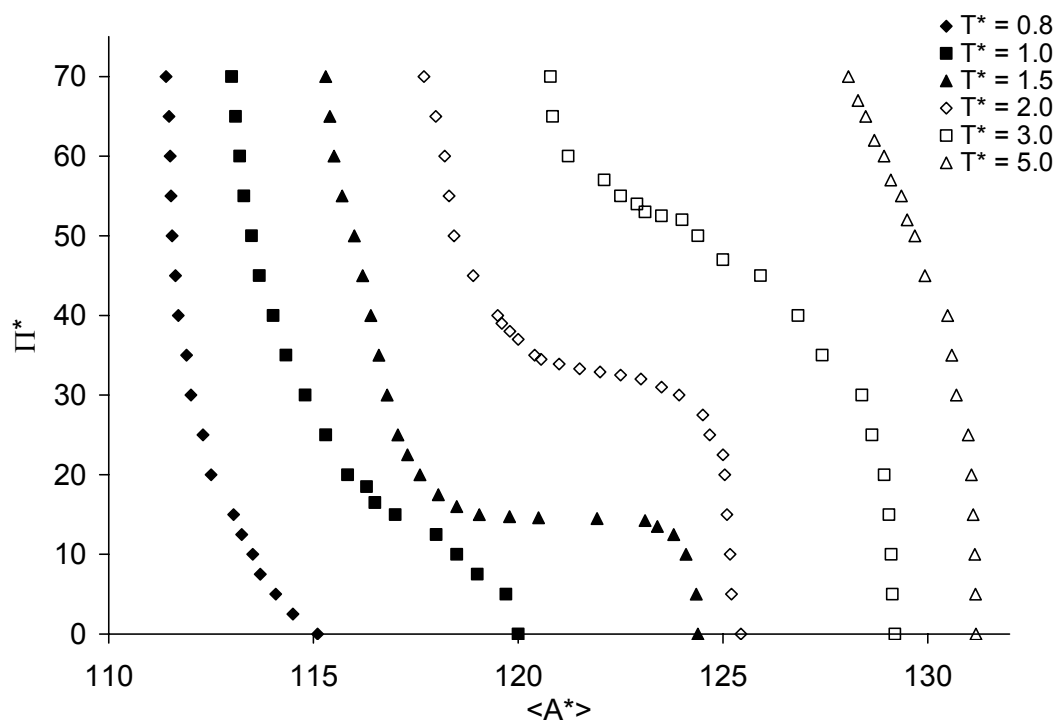


Figure 3: Lateral spreading pressure as a function of average surface area per atom at constant temperature (adsorption isotherm) for a Langmuir monolayer

monolayer changed. That behavior implies a two phase equilibrium, which in this case corresponds to LES-LCS equilibrium. It can also be observed that as expected, the equilibrium region increased as the temperature decreased. However, when the temperature decreases to  $T^*=1.0$ , the coexistence region disappears because only the LCS was stable at that temperature. Therefore, the two phase equilibrium occurred at specific pressure and temperature intervals. In all cases, visual inspection of the configurations showed that the surfactant molecules are approximately perpendicular to the water surface; parallel orientations were not observed.

The previously described phases and phase equilibrium can also be identified in Figure 4, where the average enthalpy of the surfactant molecules was computed as a function of pressure and at a fixed temperature. As expected, in all cases, as the pressure increased, the enthalpy of the system decreased and as the temperature decreased, the enthalpy decreased. For the single-phase regions, the enthalpy increased almost linearly with pressure, whereas in the coexistence region, the enthalpy remained approximately constant and as the temperature decreased, the constant region increased. Hence, the average enthalpy confirms the thermodynamic behavior observed in the isotherms.

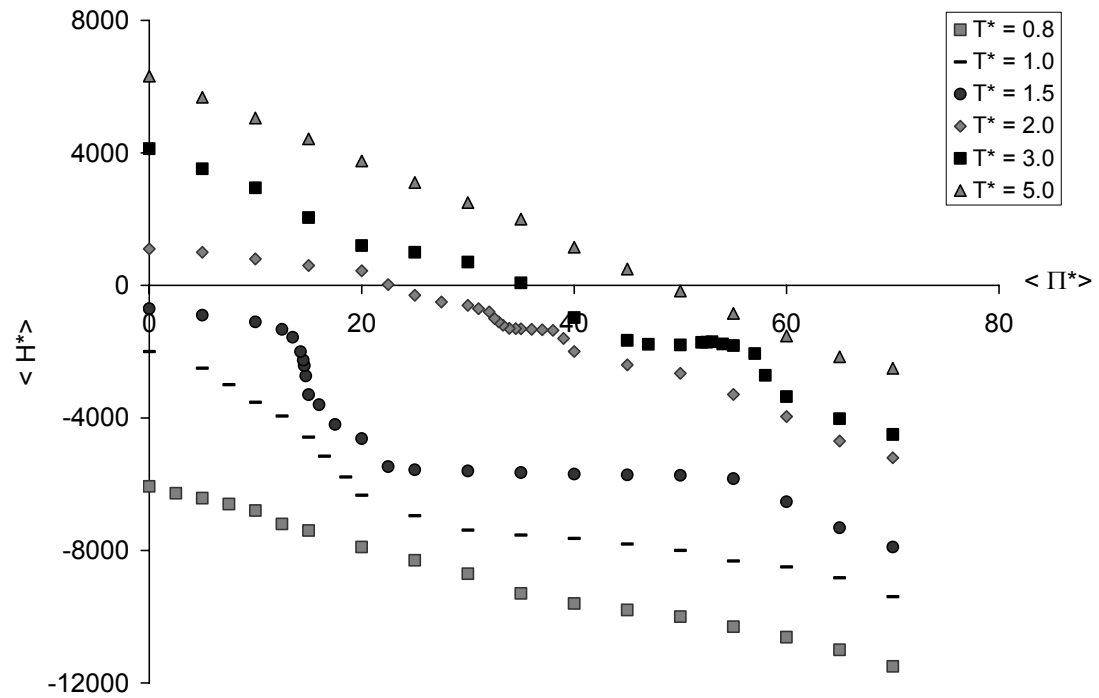


Figure 4: Average enthalpy per atom as a function of pressure at constant temperature for a Langmuir monolayer

The distribution function of distances between the surfactant molecules for a solid-like and a vapor-like surfactant monolayer is shown in Figure 5. The solid-like distribution shows a highly structured curve, while the gas-like distribution consisted of a wide single peak. The radial distribution function in Figure 6 at  $T^*=2.0$  reveals that the LES had a distribution of distance that was less structured than the solid-like arrangement but more structured than the vapor-like state. Hence, the distribution for LES was typical of a liquid. On the other hand, the distribution for the LCS was more structured than the LES, resembling a more ordered system, but not a solid-like state. Clearly, the LCS and LES obtained here were liquid in nature. In the LCS-LES coexistence region, the distribution shows peaks that correspond to LES regions and LCS regions, i.e., formation of compressed domains in a liquid expanded state.

In order to understand in a clear way the distribution function of distances previously described, Figure 7 shows snapshots of configurations typical of the LES, LCS and the LES-LCS equilibrium. This figure was constructed using the VMD software<sup>33</sup>, where only the heads of the surfactant molecules were plotted and any atom at a distance of  $1.16\sigma$  or smaller was considered a nearest neighbor and a bond was plotted. These bonds are for visual guidance only. In Figure 7(a) a compacted liquid structure can be observed, which corresponds to the LCS. This is in agreement with Figure 6 where the distribution function of

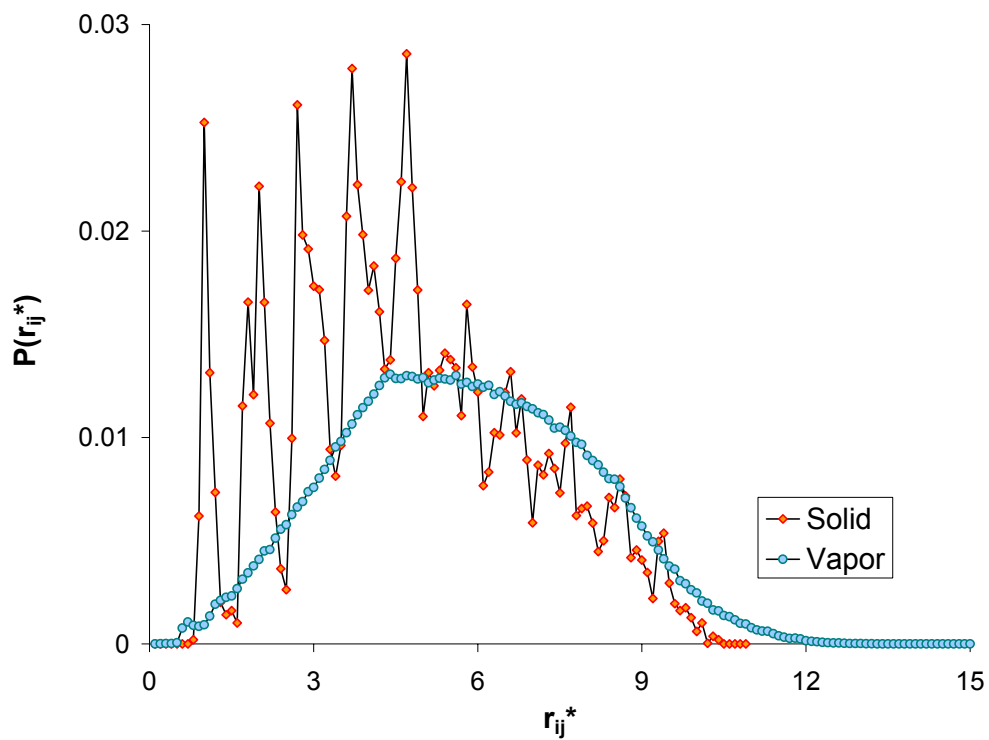


Figure 5: Distribution function of distances between pair as a function of distances between pairs of the Langmuir monolayer for a solid-like state computed at  $\Pi^* = 50$  and  $T^* = 1.0$  and for a vapor-like computed at  $\Pi^* = 1$  and  $T^* = 7.0$

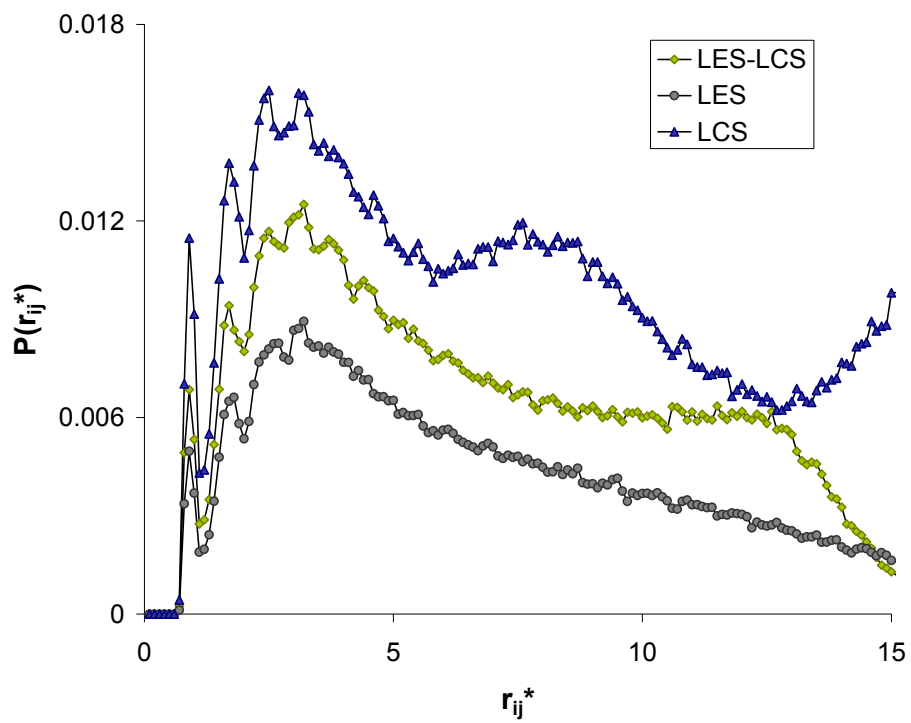


Figure 6: Distribution function of distances between pair as a function of distances between pairs of the Langmuir monolayer for the LES, LCS and the LES-LCS equilibrium computed at  $T^* = 2.0$  and  $\Pi^* = 25, 40$  and  $33$ , respectively.

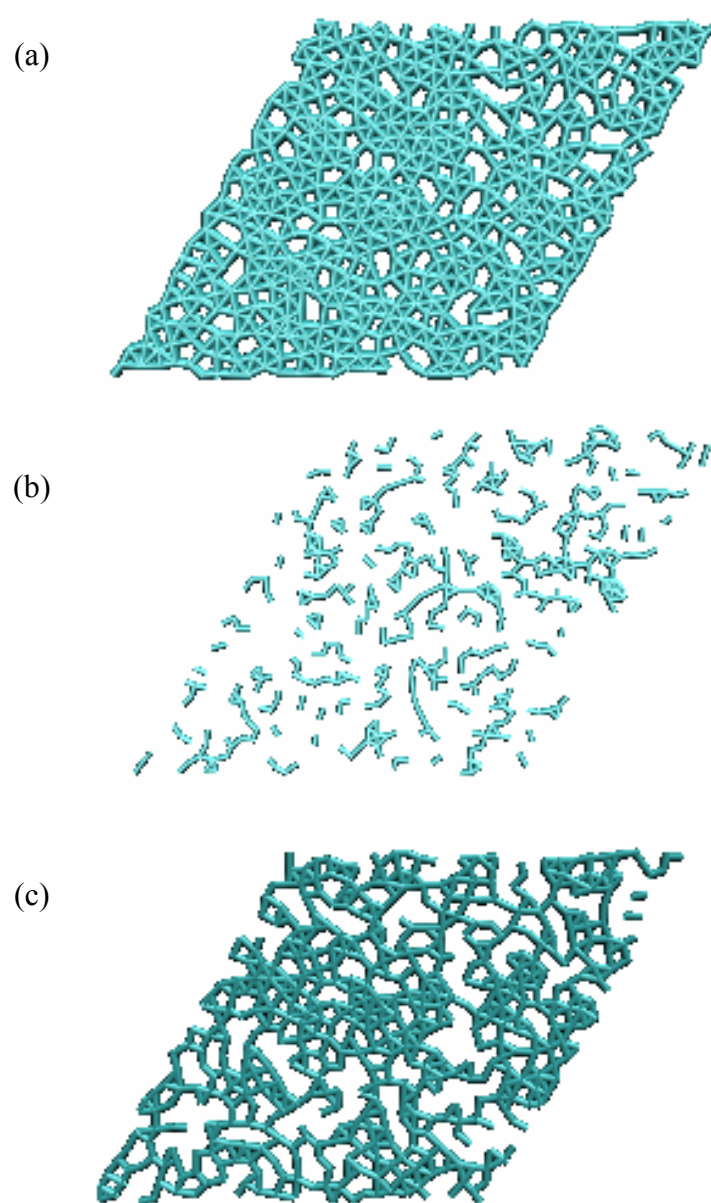


Figure 7: Snapshots of equilibrium configurations corresponding to (a) LCS, (b) LES, and (c) LES-LCS equilibrium. The snapshots were constructed plotting only the head of the surfactant molecule in the x-y plane and drawing a bond between next-nearest neighbors.

distances shows basically three peaks corresponding to the short and long range order observed in this structure. On the other hand, Figure 7(b) shows a low density system corresponding to the LES with only short range order (one peak in the radial distribution function). Finally, Figure 7(c) shows the structure of the LES-LCS equilibrium. Here compacted domains corresponding to the LCS can be identified together with less ordered region which corresponds to the LES. This diagram is consistent with the distribution of distance, where roughly two peaks can be identified; the first one associated to the distance between nearest neighbors within a domain and the second to the distance between the different domains. These snapshots are consistent with experimental data<sup>34-37</sup> obtained from atomic force and fluorescent microscopy, where compacted domains on surfactant monolayers have been identified in the LES-LCS equilibrium.

Figure 8 shows the distribution of enthalpy for  $T^* = 2.0$  at pressures of  $\Pi^* = 25, 33, \text{ and } 40$ . At the pressures where a single phase was observed,  $\Pi^* = 25$  and  $40$ , a unimodal distribution was obtained, whereas at a pressure of  $\Pi^* = 33$ , where the LES and LCS coexisted, a bimodal distribution was observed. Also, it can be observed that the LES distribution of enthalpy was wider than the LCS distribution. This was expected because the LES had many more states of different energy than the LCS, causing an increment in the width of the distribution.

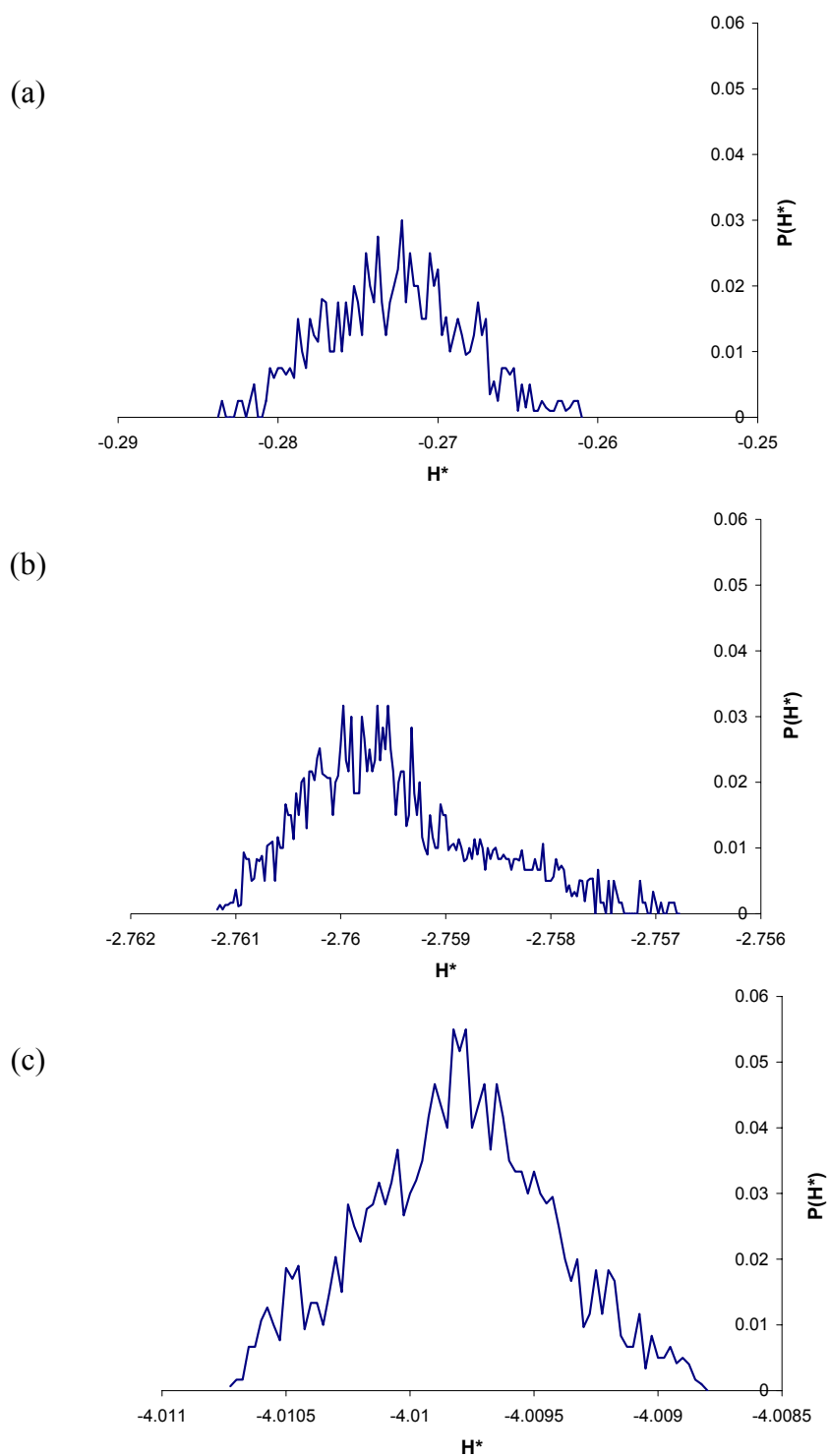


Figure 8: Distribution Function of Enthalpies as a function of enthalpies of the Langmuir monolayer at  $T^* = 2.0$  and lateral applied pressure of (a) 25 (b) 33 and (c) 40.

## 2.6 Conclusion

The equilibrium thermodynamic properties of surfactant molecules forming a Langmuir monolayer have been obtained using Monte Carlo simulations. Temperature and pressure ranges where single liquid phases are stable have been identified. These phases correspond to the LES and LCS typical of surfactant molecules forming a Langmuir monolayer in presence of an applied external pressure. A two-phase coexistence region corresponding to the LES-LCS equilibrium was identified by means of adsorption isotherms, average enthalpies and various distribution functions. The results obtained are in qualitative agreement with experimental studies<sup>3, 11-13</sup> of Langmuir monolayers using Langmuir trough balance experiments. Finally, the model used leads to a simple but qualitatively correct description of the Langmuir monolayer thermodynamic properties.

## **Chapter 3**

### **Langmuir Monolayer Critical Properties Determination**

#### **Model and Simulation Details**

In order to identify Langmuir monolayer critical points for the LES-LCS and LES-V phase coexistence, a Standard Virtual Gibbs ensemble (SVGE) Monte Carlo simulation was performed. Phase diagrams of temperature versus phase density, known as Cailletet–Mathies phase diagrams, were constructed for both phase equilibria at three different interaction values between the surfactant molecules and the aqueous phase. Furthermore, the Ising model and the rectilinear law were implemented in order to determine the critical temperature and the critical density for both phase equilibrium, respectively.

## 3.1 Model

### 3.1.1 Interparticle Potential

Surfactant molecules were modeled by one bead representing the hydrophilic head and three beads representing the hydrophobic tail. The intermolecular forces between particles are described using two bead-like models<sup>27</sup>. All interactions between adjacent particles forming a surfactant molecule were described by harmonic oscillators of the form:

$$V_b(r_{ij}^a) = \frac{K}{2}(r_{ij} - \sigma)^2 \quad (12)$$

K is the force constant set to 500 units,  $r_{ij}$  is the distance between adjacent beads i and j, and  $\sigma$  is the equilibrium distance between beads, which was set to 1.0. The non-bonding interactions between surfactant molecules were modeled using a modified Lennard-Jones (L-J 12-6) potential<sup>24</sup> of the form:

$$\frac{V_{nb}(r_{ij})}{4\epsilon_{ij}} = R_{ij} \left( \frac{\sigma_{ij}}{r_{ij}} \right)^{12} - A_{ij} \left( \frac{\sigma_{ij}}{r_{ij}} \right)^6 \quad (13)$$

where  $V_{nb}(r_{ij})$  is the potential energy between beads i and j that are at a separation denominated  $r_{ij}$ . The parameter  $\epsilon_{ij}$  defines energy and  $\sigma_{ij}$  defines length units and their values were fixed to 1.0 and 0.8, respectively. As in the first part of this work, the constants  $R_{ij}$  and  $A_{ij}$  are used to modify the repulsive and attractive parts of the potential, respectively, and are defined in Table 1.

The water phase was modeled as a continuous surface using the 9-3 Lennard-Jones Potential<sup>32</sup> of the form:

$$\frac{V_S(r_Z)}{4\varepsilon_Z} = R_S \left( \frac{\sigma_S}{r_Z} \right)^9 - A_S \left( \frac{\sigma_S}{r_Z} \right)^3 \quad (14)$$

Thus, the water phase will be referred hence forth as the surface. In equation 14 the  $V_S(r_Z)$  is the potential energy and  $r_Z$  is the distance between the surfactant molecules and the surface. The value of  $\sigma_S$  was fixed to 1.0, but in this case, the value of  $\varepsilon_S$  was varied in order to increase the interaction between the surfactant molecules and the aqueous phase. The values used were 1, 10, and for the strongest interaction 50.

### 3.2 Method

The critical properties of the phase equilibrium between the LES-LCS and LES-V phases of the Langmuir monolayer were modeled using the Metropolis Monte Carlo algorithm extended to the Standard Virtual Gibbs ensemble (SVGE) where the number of particles, the temperature and the volume (NVT ensemble) are held constant. The moves employed in the simulation were particle displacement and changes in volume of the surfactant monolayer. Details on the method are given in the next section.

### 3.2.1 Monte Carlo Technique in the SVGE

Standard Virtual Gibbs ensemble<sup>32</sup> (SVGE), a class of Monte Carlo methods, was used in this work to simulate phase equilibrium between two equilibrium phases for a model Langmuir monolayer. In this ensemble two simulation boxes are defined, where each phase occupies one and there is no particle transfer allowed between them.

It is known that by removing the mass–volume balance constraints of conventional Gibbs ensembles, the resulting SVGE can be used to effectively simulate systems wherein two types of moves are performed in order to maintain thermodynamic equilibrium. First, particles displacements (thermal equilibrium), and second, volume changes (mechanical equilibrium). In the present study the total system (both boxes) was kept at constant number of particles, temperature, and volume (NVT). The initial choices for the volume and number of particles would not permit direct methods to achieve convergence to a stable two-phase state.

As in the Gibbs ensemble, in the SVGE the probability of acceptance was calculated as the product of the probability of acceptance for each box, i.e.  $a = a_I a_{II}$ , where  $a_I$  and  $a_{II}$  are the acceptance probabilities for a certain move performed in box I and II, respectively. Then, for particles displacement the acceptance probability is given by

$$a(q_f, q_i) = \exp[-\beta(\Delta U_I + \Delta U_{II})] \quad (15)$$

Here  $\Delta U_I$  and  $\Delta U_{II}$  are the difference in configurational energy due to particle displacement in boxes I and II, respectively.

In the case of volume changes, in order to maintain the total volume constant, the volume of box I is increased by  $\Delta V$  and the volume of box II decreased by  $\Delta V$ . Hence, the acceptance probability for volume variations is

$$a(q_f, q_i) = \exp \left[ -\beta [(\Delta U_I + \Delta U_{II}) - \frac{N_I}{\beta} \ln \frac{V_I + \Delta V}{V_I} - \frac{N_{II}}{\beta} \ln \frac{V_{II} - \Delta V}{V_{II}}] \right] \quad (16)$$

where  $V_I$  and  $V_{II}$  are the volumes of boxes I and II, respectively.  $N_I$  and  $N_{II}$  are the number of particles in boxes I and II, respectively.

### 3.3 Simulation Details

As stated, each simulation was performed in the Standard Virtual Gibbs Ensemble where two rhombic boxes were defined, each containing one phase. The initial sizes of the boxes in the x-y plane were 40.63 and 400 reduced units for the liquid and vapor phases, respectively. A total of 400 surfactant molecules were used in each simulation box. Each surfactant molecule is composed of one bead representing the hydrophilic head and three identical beads representing the hydrophobic tail. The starting configuration used for the surfactant molecules placed the beads in a straight line separated at a distance of  $1.0 \sigma_{ij}$  and they rested on the lower wall over the x-y plane.

Each simulation was run for a total of  $10^6$  warm-up moves and  $10^6$  moves were data were collected with uncertainties calculated to one standard deviation. The particles were moved using a Metropolis box size such that 50% of the moves were accepted. After every Monte Carlo step a volume change was allowed with a step size such that 30% of the changes were accepted. Periodic Boundary Conditions in the x and y directions were implemented for the surfactant monolayer.

### 3.4 Results and Discussion

Figures 9 to 15 show the results obtained using the SVGE for the system described in Section 3.3. As shown in Figure 9, Caillette-Matties phase diagrams were constructed for all the interactions between the surfactant molecules and the surface studied for  $\epsilon = 1, 10, \text{ and } 50$ . This figure also shows that at low values of average phase density ( $\langle \rho^* \rangle$ ) we found the monolayer in a vapor like state in equilibrium with the LES state. When the average phase density increases, the equilibrium observed in the diagram occurs between the LES-LCS of the monolayer. When the monolayer is in the vapor phase, the attraction between the surfactant molecules and the surface is weak (due to high value of the system volume), therefore the magnitude of the interaction between them does not affect their individual density values and furthermore, density values will be similar among them.

The LES-V and LES-LCS transition lines merge at low temperatures and then the phase diagram equilibrium line ascends to the phase equilibrium critical point. Fluorescence microscopy studies of the LES-LCS coexistence region of pentadecanoic acid on acidified water reveal that when the temperature is lowered, circular domains appear on the LES state. These domains have been attributed to the monolayer LCS phase<sup>38</sup>. This behavior implies that as for the LES- V equilibrium, the LES-LCS coexistence curve ends in a critical point. As yet, the value of this critical point has not been determined experimentally or theoretically<sup>3</sup>.

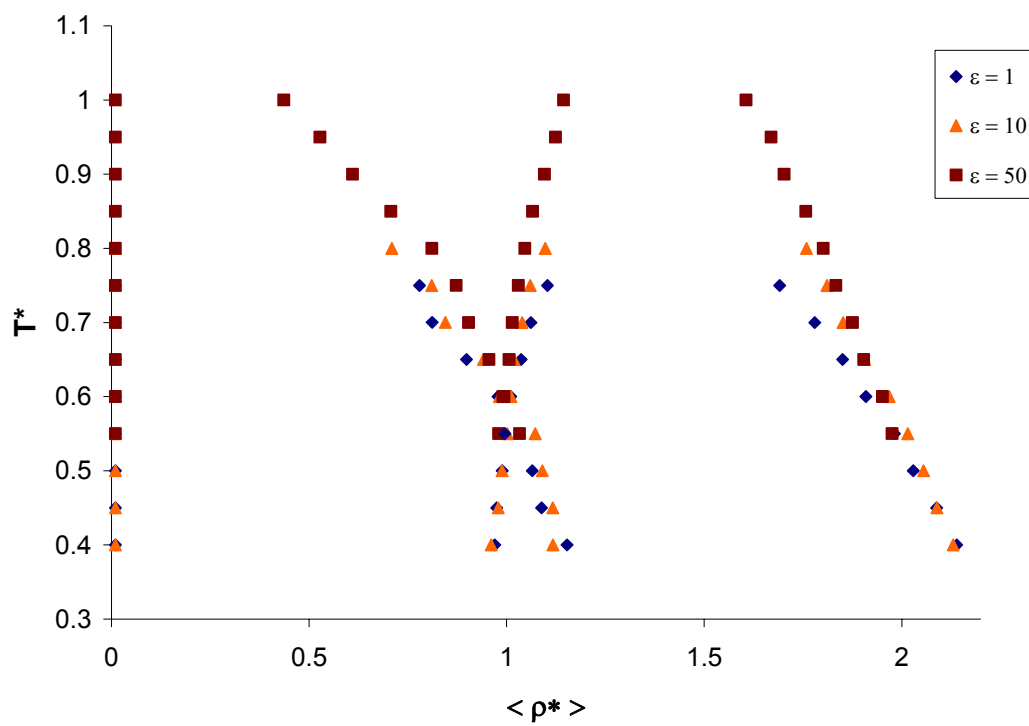


Figure 9: Caillette-Matties phase diagram for the Langmuir monolayer at three different interaction values.

In order to obtain the critical properties for the equilibrium between LES-LCS and LES-V states, similar procedures found in previous studies have been used<sup>39-43</sup>. Specifically, it has been extensively discussed that the form of the Cailleite-Matties curve obeys the Ising model<sup>39</sup>, which has the form:

$$T^* = a(\rho_1 - \rho_2)^\beta + T_c \quad (17)$$

where  $\rho_1$  and  $\rho_2$  are the equilibrium densities for the phases under study, i.e. for the study of the equilibrium between the LES-LCS phases,  $\rho_1$  corresponds to the LCS, whereas  $\rho_2$  corresponds to the LES state. In this expression  $\beta$  is the critical exponent and its value was set to 3 due to empirical data<sup>40</sup>, and  $T_c$  is the critical temperature. To calculate the critical density,  $\rho_c$ , the rectilinear law<sup>39</sup> was used

$$\frac{\rho_1 + \rho_2}{2} = a(T^* - T_c) + \rho_c \quad (18)$$

Figures 10 to 12 show the implementation of equation 17 and 18 for the LES-LCS equilibrium at three different interactions between the surfactant molecules and the aqueous phase. The critical temperature determined for  $\varepsilon$  value of 1.0 was  $T_c^* = 0.79 \pm 0.01$ . Meanwhile, for an  $\varepsilon$  value of 10 and 50, the critical temperature calculated was  $T_c^* = 0.87 \pm 0.01$  and  $T_c^* = 1.01 \pm 0.01$ , respectively. The critical density for the LES-LCS equilibrium was found to be  $1.38 \pm 0.00$ ,  $1.39 \pm 0.01$ ,  $1.38 \pm 0.00$  for  $\varepsilon$  value of 1.0, 10 and 50, respectively.

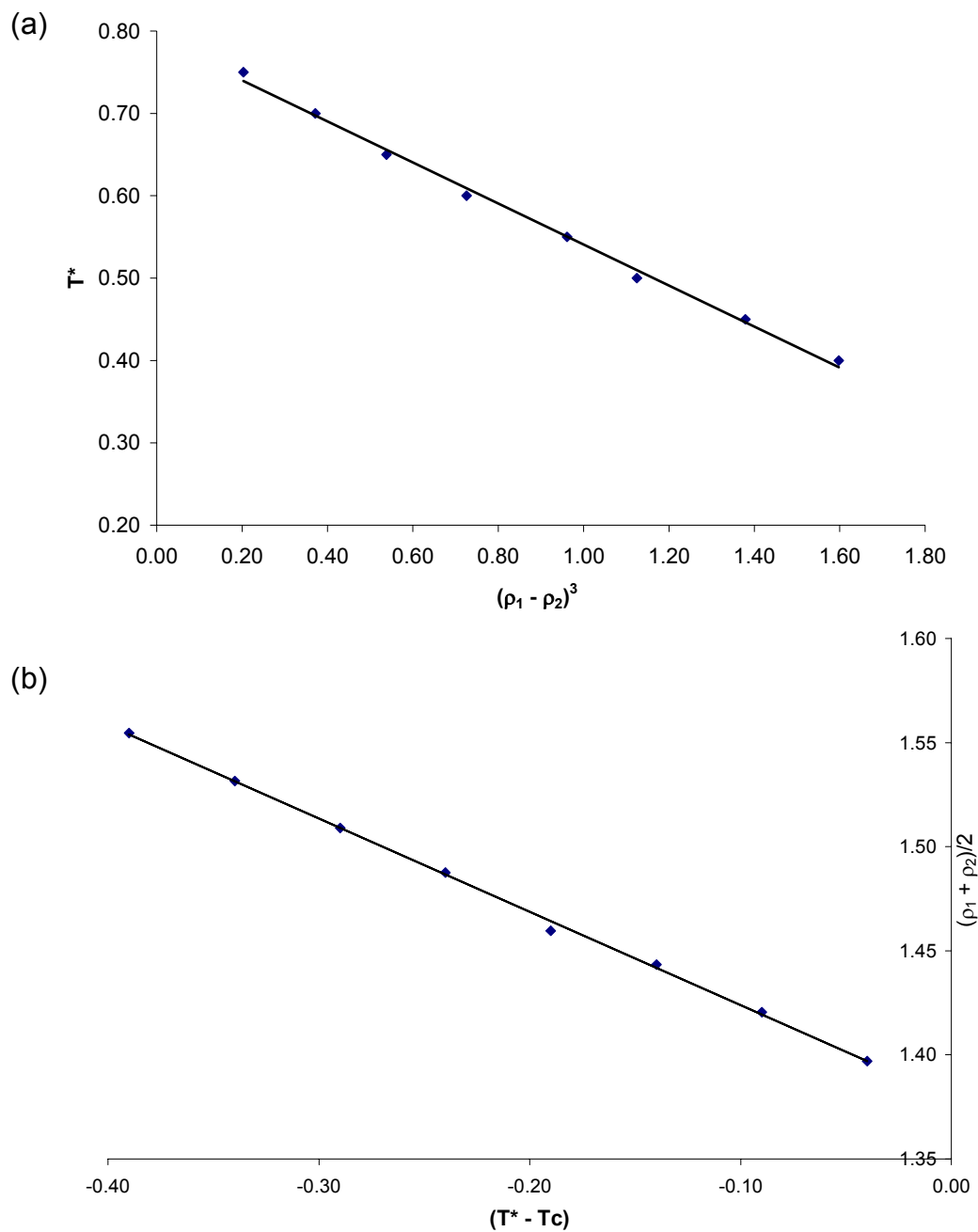


Figure 10: For  $\varepsilon = 1$  (a) Reduced temperature as a function of  $(\rho_1 - \rho_2)^3$  for the LES-LCS equilibrium (b) Rectilinear law implementation for the critical density identification. The straight line represents a least-square fit to the simulation results.

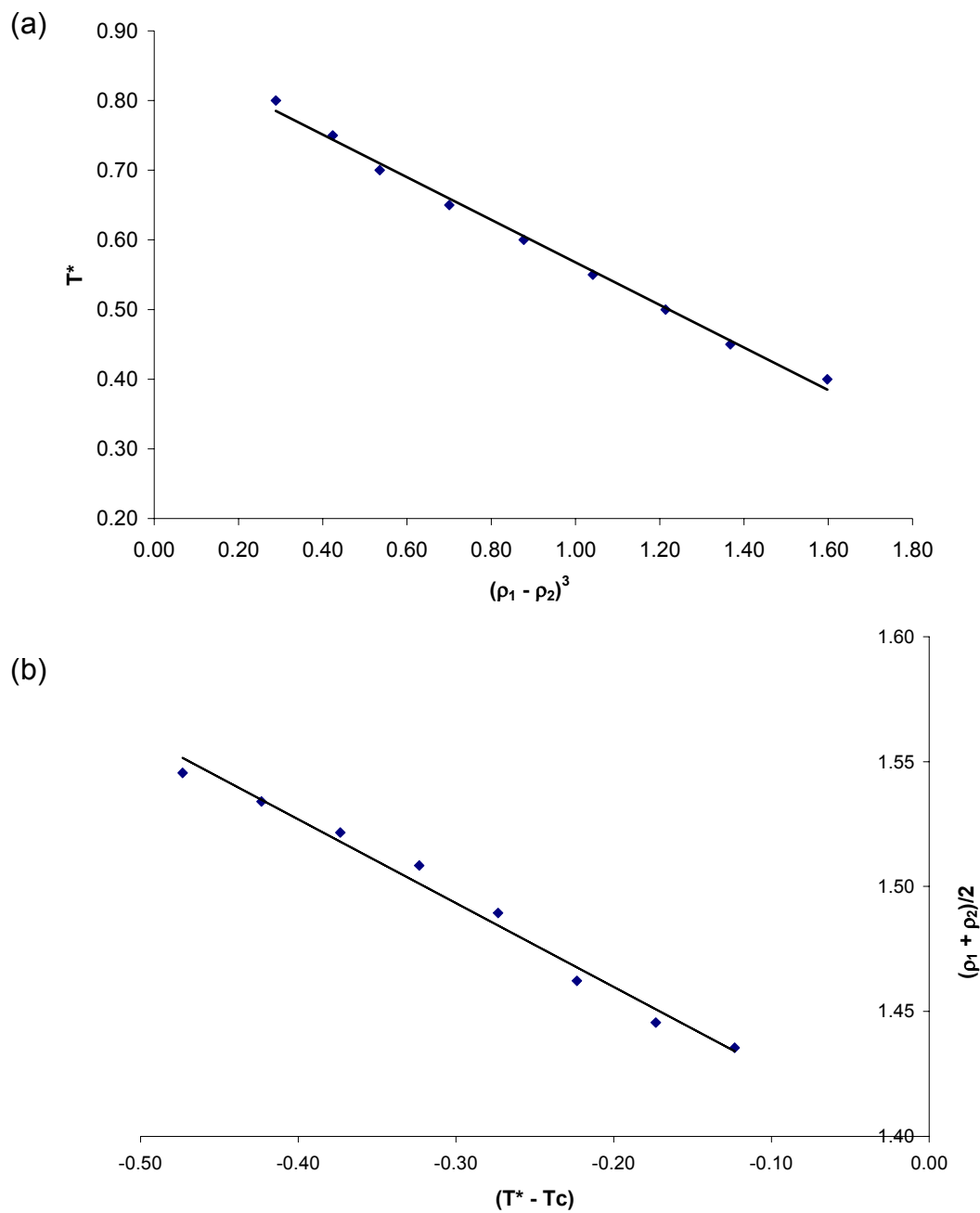


Figure 11: For  $\varepsilon = 10$  (a) Reduced temperature as a function of  $(\rho_1 - \rho_2)^3$  for the LES-LCS equilibrium (b) Rectilinear law implementation for the critical density identification. The straight line represents a least-square fit to the simulation results.

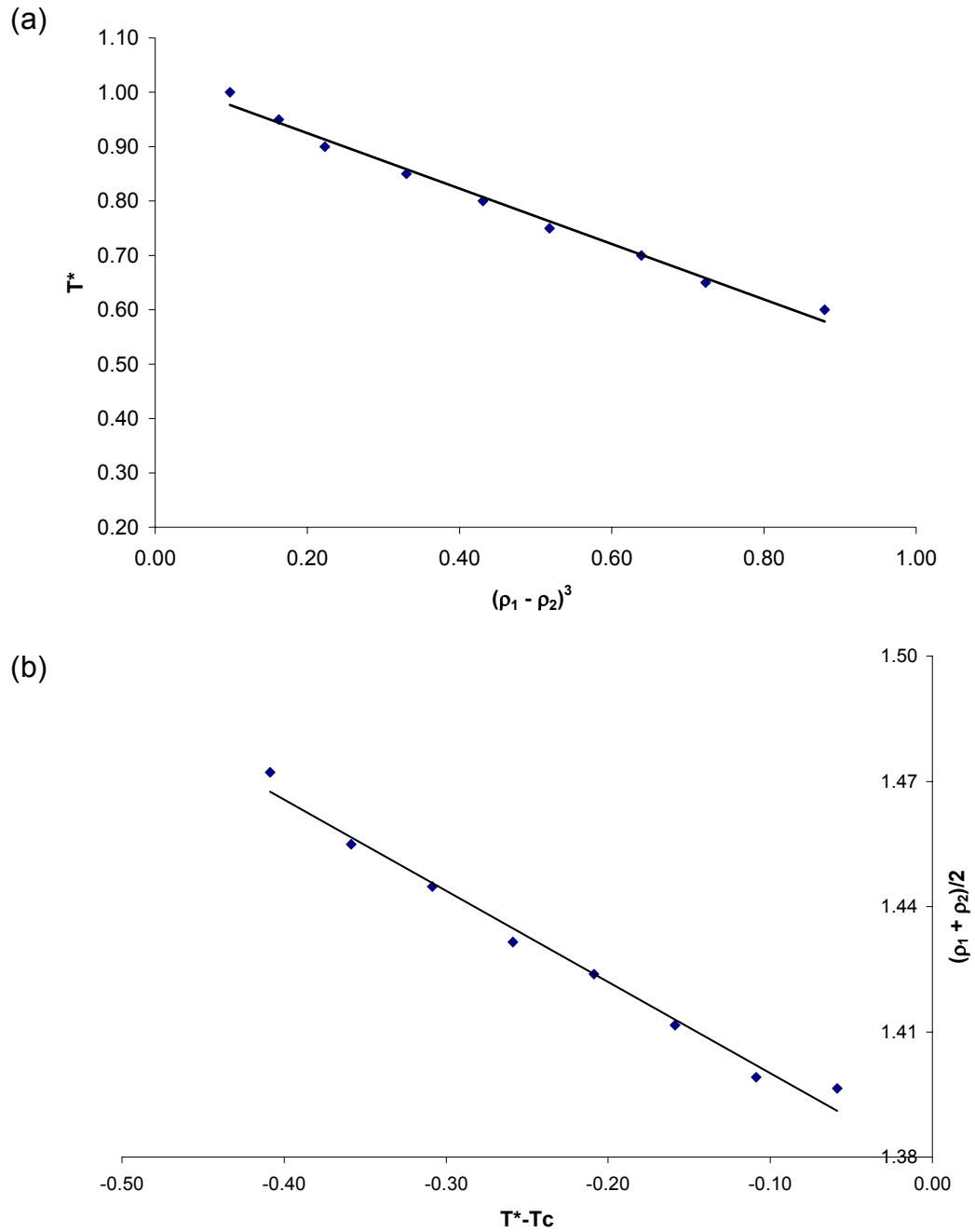


Figure 12: For  $\varepsilon = 50$  (a) Reduced temperature as a function of  $(\rho_1 - \rho_2)^3$  for the LES-LCS equilibrium (b) Rectilinear law implementation for the critical density identification. The straight line represents a least-square fit to the simulation results.

The critical temperature and critical density for the equilibrium between the LES-V of the monolayer, were obtained in the same way as was the LES-LCS equilibrium; by using equation 17 and 18. Figures 13 to 15 show the graphs constructed for the determination of the aforementioned parameters. The critical temperature for an  $\varepsilon$  value of 1.0 was  $T_c^* = 0.91 \pm 0.01$ ; while for an  $\varepsilon$  value of 10 and 50, the obtained critical temperature was  $T_c^* = 0.92 \pm 0.01$  and  $T_c^* = 1.01 \pm 0.01$ , respectively. The critical densities for the LES-V equilibrium were found to be  $0.28 \pm 0.01$ ,  $0.28 \pm 0.01$ , and  $0.26 \pm 0.02$  for  $\varepsilon$  values of 1.0, 10 and 50, respectively.

Table 2 summarizes the results obtained for the LES-LCS and LES-V equilibrium. It has been shown that an increase in the interaction strength between surfactant molecules and the aqueous phase leads to more condensed monolayers<sup>43-44</sup>. As expected, the system's critical temperature is directly proportional to the magnitude of the interaction. It is also observed that the critical temperature is higher for the LES-V equilibrium than for the LES-LCS equilibrium because a higher energy is required to reach the coexistence state. Our results also indicate that since the critical density values only depend on the number of particles and system volume, these values remain approximately constant, regardless of the interaction strength.

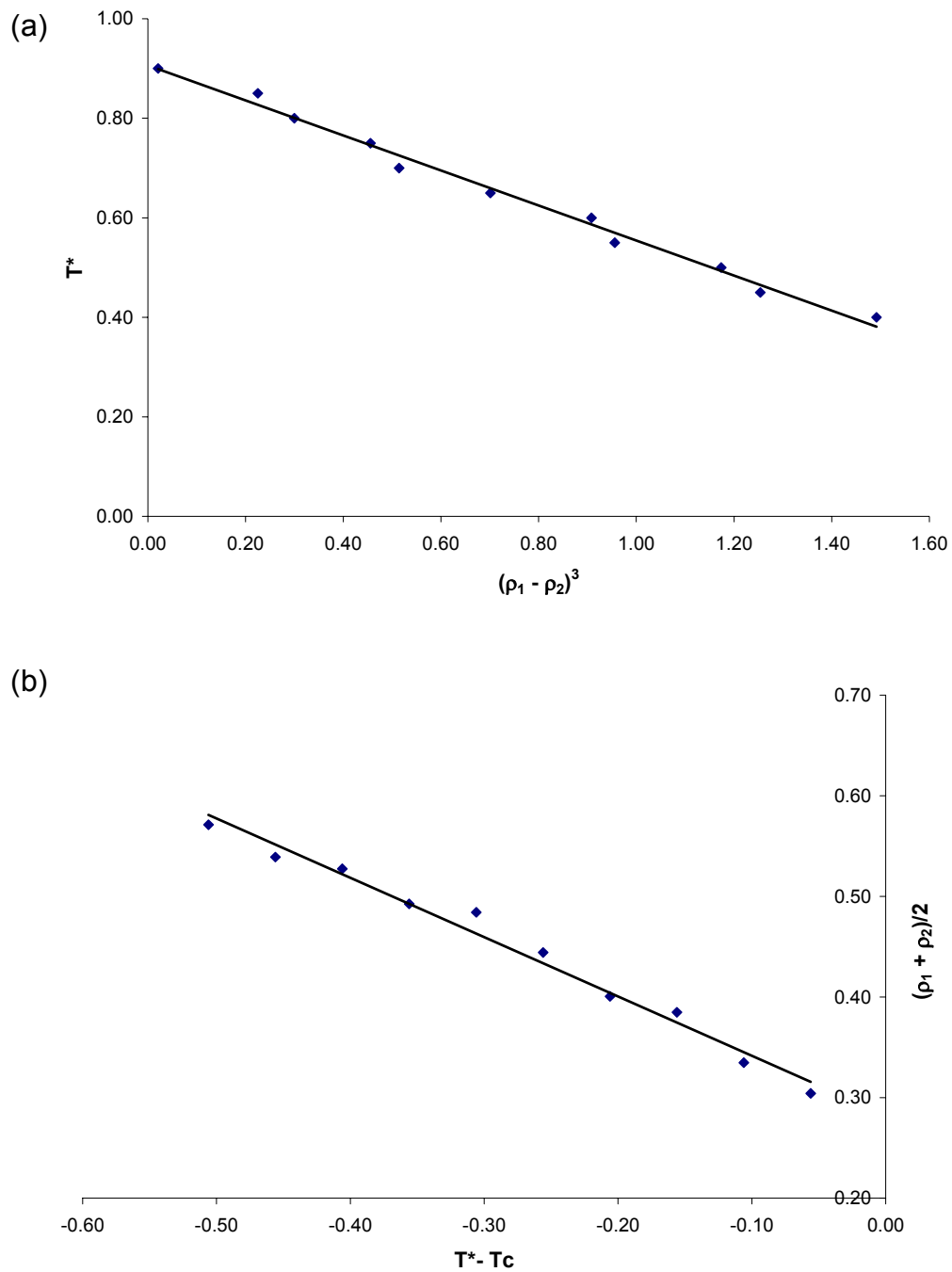


Figure 13: For  $\varepsilon = 1$  (a) Reduced temperature as a function of  $(\rho_1 - \rho_2)^3$  for the LES-V equilibrium (b) Rectilinear law implementation for the critical density identification. The straight line represents a least-square fit to the simulation results.

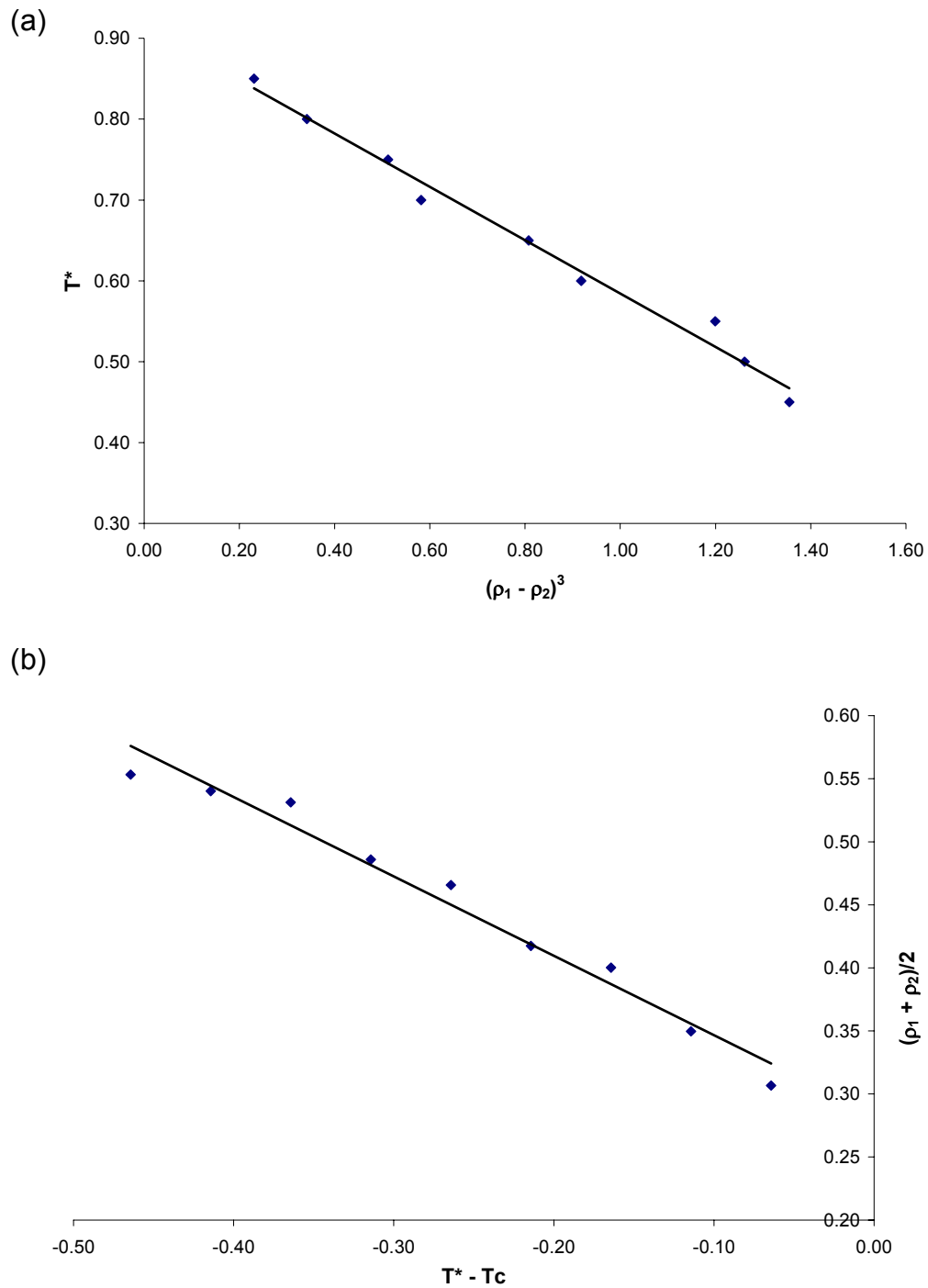


Figure 14: For  $\varepsilon = 10$  (a) Reduced temperature as a function of  $(\rho_1 - \rho_2)^3$  for the LES-V equilibrium (b) Rectilinear law implementation for the critical density identification. The straight line represents a least-square fit to the simulation results.

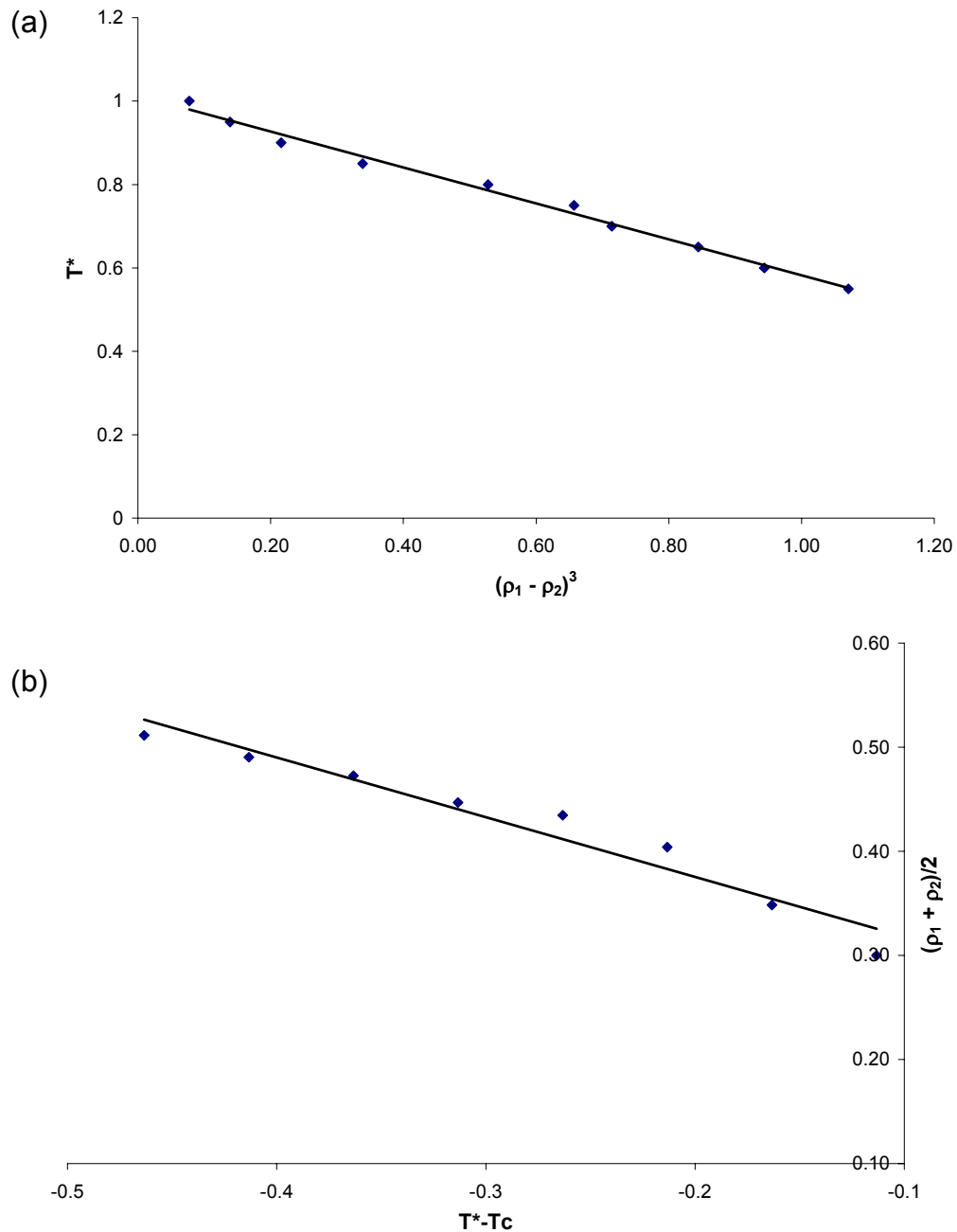


Figure 15: For  $\varepsilon = 50$  (a) Reduced temperature as a function of  $(\rho_1 - \rho_2)^3$  for the LES-V equilibrium (b) Rectilinear law implementation for the critical density identification. The straight line represents a least-square fit to the simulation results.

$\varepsilon$	LES- LCS Equilibrium		LES-V Equilibrium	
	$T_c^*$	$\rho_c^*$	$T_c^*$	$\rho_c^*$
<b>1</b>	0.79±0.01	1.38±0.00	0.91±0.01	0.28±0.01
<b>10</b>	0.87±0.01	1.39±0.01	0.92±0.01	0.28±0.01
<b>50</b>	1.01±0.01	1.38±0.00	1.01±0.01	0.26±0.02

Table 2: Langmuir Monolayer critical properties for the LES-LCS equilibrium and the LES-V equilibrium. The critical temperature and density are reported in reduced units.

### 3.5 Conclusion

The critical point of the LES-LCS and LES-V equilibrium for a Langmuir monolayer has been identified using Monte Carlo simulations in the Standard Virtual Gibbs ensemble. The Caillete-Mathias phase diagrams were constructed for the identification of the critical temperature ( $T_c^*$ ) and critical density ( $\rho_c^*$ ). The identification of the critical point was obtained by implementing the Ising Model and the rectilinear approximation. At this critical state the densities of both phases under study become closer to each other until the critical temperature is reached where the two densities are equal and the phase boundary disappears.

It was shown that the interaction strength between the surfactant molecules and the surface affects the values of the critical temperature, but not the critical density, for both the LES-LCS and for the LES-V equilibrium. The critical temperature value increases with increments in the interaction between the surface and the surfactant molecules. Furthermore, the density values for both phase equilibriums are independent of the interaction value between the surfactant molecules and the aqueous sub-phase. Finally, the Monte Carlo ensemble implemented leads to a proper qualitative identification of the critical properties for the LES-LCS and the LES-V equilibrium for a model Langmuir monolayer.

## Chapter 4

### General Conclusions

The structure and phase transition in Langmuir monolayers can be modeled by means of computer simulation using models which include all the system's atoms or using simplified molecular models. Complex materials like surfactant layers and polymer mixtures require the use of simplified models denominated as coarse-grained<sup>45</sup>. Using coarse-grained potentials we have achieved a basic physical understanding of a model Langmuir monolayer.

It is known that single component Langmuir monolayers can undergo one liquid-liquid phase transition. In this study, the equilibrium between two liquid phases of a Langmuir monolayer was identified by means of adsorption isotherms, average enthalpies and various distribution functions. The temperature and pressure range where single liquid phases are stable were also identified. In general, the behavior of monolayers formed by alcohols, esters, or phospholipids is qualitatively similar<sup>46</sup>. Due to the behavior of these monolayers we can conclude that even though our models did not take into account the

specific atoms that compose the system, our results are in qualitative agreement with earlier theoretical predictions and experimental data.

As mentioned in section 3.5, the LES-LCS coexistence curve has a critical point. It is also known, that the monolayer-subphase interactions can be widely varied by changing the pH or ionic content of the subphase<sup>6</sup>. In this study, the critical temperature and density for the LES-LCS and LES-V equilibrium was determined varying the interaction strength between surfactant molecules and the subphase. Our results suggest that the system's critical temperature is directly proportional to the magnitude of the interaction, while the density values for both phase equilibriums are independent of the interaction strength.

Finally, the implemented ensemble methodologies lead to a simple but qualitatively correct description of the Langmuir monolayer thermodynamic and critical properties. Such knowledge is important, not only for a better physical understanding, but also to help design new ones with appropriate characteristics for specific applications.

## References

1. M. J. Rosen, *Surfactants and Interfacial Phenomena*, 2<sup>nd</sup> ed; John Wiley and Sons: 1989; p 1.
2. S. Schurch, M. Lee, and P. Gehr, *Pure and Appl. Chem.*, **64**, 1745 (1992).
3. M. Jones and D. Chapman, *Monolayer. Micelles, Monolayer and Biomembranes*; Wiley, New York (1995)
4. M. S. Kent, H. Yim, and D. I. Sasaki, *Langmuir*. **18**, 3754 (2002).
5. M.S. Tomassone, A. Couzis, C.M. Maldarelli, J.R. Banavar, and J. Koplik, *J. Chem. Phys.* **115**, 8634 (2001).
6. V. Kaganer, H. Möhwald, and P. Dutta, *Rev. Mod. Phys.* **71**, 779 (1999).
7. S.B. Opps, B. Yang, C. Gray, and D. Sullivan, *Phys. Rev.* **63**, 41602 (2001).
8. K. A. Suresh and A. Bhattacharyya, *J of Phys.* **53**(1), 93 (1999).
9. A. Polimeno, R. Marijin, and Y. Levine, *J. Chem. Phys.* **115**, 6185 (2001).
10. Shin S., Zhen-Ghang W., and S. Rice, *J. Chem. Phys.* **92**, 1427 (1989).
11. S. Ramos, S and R. Castillo, *J. Chem. Phys.* **110**, 7021 (1999).
12. C. Lautz, Th. M. Fisher, and J. Kildea, *J. Chem. Phys.* **106**, 7448 (1997).
13. E. Teer, C. Knobler, C. Lautz, S. Wurlitzer, J. Kildae, and Th. M. Fisher, *J. Chem. Phys.* **106**, 1913 (1997).
14. J. Buontempo, and S. Rice, *J. Chem. Phys.* **99**, 7030 (1993).
15. B. Lin, B. Peng, J.B. Ketterson, P. Dutta, B. N. Thomas, J. Buontempo, and S. Rice, *J. Chem. Phys.* **90**, 2393 (1988).
16. I. R. Peterson, R.Brzezinski, M. Kenn, and R. Steitz, *Langmuir*. **8**, 2995 (1992).
17. A. Flores, S. Ramos, P. Ize, and, R. Castillo, *J. Chem. Phys.* **119**, 5644 (2003).

18. S.B. Opps, B.G. Nickel, C.G. Gray, and D. Sullivan, *J. Chem. Phys.* **113**, 339 (2000).
19. M.S. Tomassone, A. Couzis, C.M. Maldarelli, J.R. Banavar, and J. Koplik, *J. Chem. Phys.* **115**, 8634 (2001).
20. C. Stadler and F. Schmid, *J. Chem. Phys.* **110**, 9697 (1999).
21. S. Paddeu, M. Kumar Ram, *Nanotechnology.* **9**, 228 (1998)
22. H. Tachibana, Y. Yamanaka, and M. Matsumoto, *J. Mater. Chem.* **12**, 938 (2002).
23. F. Muller, and P. Fontaine, *Langmuir.* **20**, 4791 (2004)
24. M.P. Allen, and D.J. Tildesly, *Computer Simulation of Liquids.* (Clarendon Press, Oxford, 1987).
25. V. Ortíz, J. R. Maury-Evertsz, and G.López, *Chem. Phys. Lett.* **368**, 452 (2003).
26. J. Potoff and A. Z. Panagiotopoulos, *J. Chem. Phys.* **109**, 10914 (1998).
27. Y.J. Sheng, A. Panagiotopoulos, S.K. Kumar, and I. Szleifer, *Macromolecules* **27**, 400 (1994).
28. M. Ocasio, J.R. Maury-Evertsz, B. Pastrana-Ríos, and G.E. López, *J. Chem. Phys.*, **119**, 9274 (2003).
29. D. S. Corti *Molec. Phys.*, 100, 1887 (2002)
30. M. Ocasio, and G. López, *Chem. Phys. Lett.* **356**, 168 (2002).
31. M. Vicéns, and G. López, *Phys. Rev. A* 62, 033203 (2000).
32. B. Smit and S. Frenkel, *Understanding Molecular Simulations* (Academic Press, 2001)

33. Visual Molecular Dynamics (VMD)—This work was supported by the Theoretical and Computational Biophysics group, a NIH Resource for Macromolecular Modeling and Bioinformatics, at the Beckman Institute, University of Illinois at Urbana-Champaign.
34. J. Mikrut, P. Dutta, J. B. Ketterson, and R. C Mac-Donald, *Phys. Rev. B* **48**, 14479 (1993).
35. K. Nag, J. Perez-Gil, M. L. Ruano, L. A. Worthman, J. Steward, C. Casals, and K. M. Keough, *Biophys. J.* **74**, 2983 (1998).
36. K. Nag, J. S. Pao, R. R. Harbottle, F. Possmayer, N. O. Peterson, and L. A. Bagatolli, *Biophys. J.* **82**, 2041 (2002).
37. J. Bernardino de la Serna, J. Perez-Gil, A. Simonsen, and L. A. Bagatolli, *Biophys. J.* **279**, 40715 (2004).
38. J. Harris, S. A. Rice, *J. Chem. Phys.* **89**, 5898 (1988).
39. J. J. Potoff and A. Z. Panagiotopoulos, *J. Chem. Phys.* **109**, 10914 (1998).
40. B. Smit, *J. Chem. Phys.* **96**, 8639 (1992).
41. B. Smit and D. Frenkel, *J. Chem. Phys.* **94**, 5665 (1991).
42. R. R. Singh, K. S. Pitzer, J. J. De Pablo, and J. M. Prausnitz, *J. Chem. Phys.* **92**, 5463 (1990).
43. C. A. Helm, L. Laxhuber, M. Loosche, H. Mohwald, *Colloid Polym. Sci.* **264**, 46 (1986).
44. K. A. Riske, M. J. Politi, W. F. Reed, M. T. Lamy-Freund, *Chemistry and Physics of Lipids*, **89**, 31 (1997).
45. K. Binder, M. Müller, and F. Schmid, *Computing in Science and Engineering*, 12 (1999).
46. C. Stadler, H. Lange, and F. Schmid, *Physical Review E*, **59**, 4248, (1999).